Structural Changes in Iron Oxide and Gold Catalysts during Nucleation of Carbon Nanotubes Studied by *In Situ* Transmission Electron Microscopy

Dai-Ming Tang,[†,‡,§] Chang Liu,[†,*] Wan-Jing Yu,[†] Li-Li Zhang,[†] Peng-Xiang Hou,[†] Jin-Cheng Li,[†] Feng Li,[†] Yoshio Bando,[§] Dmitri Golberg,[§,*] and Hui-Ming Cheng[†]

[†]Shenyang National Laboratory for Materials Science, Institute of Metal Research, Chinese Academy of Sciences, 72 Wenhua Road, Shenyang 110016, China, and [‡]International Center for Young Scientists (ICYS), [§]World Premier International (WPI) Center for Materials Nanoarchitectonics (MANA), National Institute for Materials Science (NIMS), Namiki 1—1, Tsukuba, Ibaraki, 305—0044, Japan

ABSTRACT We report a simple, versatile *in situ* transmission electron microscopy (TEM) approach for investigating the nucleation and growth mechanism of carbon nanotubes (CNTs), by which the composition, phase transition, and physical state of various catalysts can be clearly resolved. In our approach, catalyst nanoparticles (NPs) are placed in a multiwall CNT "tubular furnace" with two open ends, and a high temperature is obtained by Joule heating in the specimen chamber of a TEM. The carbon is supplied by electron irradiation-induced injection of carbon atoms. Comparative studies on the catalytic behavior of traditional iron oxide and recently discovered gold catalysts were performed. It was found that the growth of CNTs from iron oxide involves the reduction of Fe_2O_3 to Fe_3C, nucleation and growth of CNTs from partially liquefied Fe_3C, and finally the formation of elemental Fe when the growth stops. In contrast, while changes in shape, size, and orientation were also observed for the fluctuating Au NPs, no chemical reactions or phase transitions occurred during the nucleation of CNTs. These two distinct nucleation and growth processes and mechanisms would be valuable for the structure-controlled growth of CNTs by catalyst design and engineering.

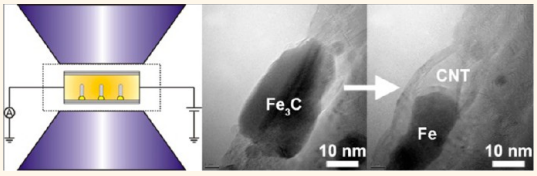

KEYWORDS: carbon nanotube · nucleation · growth mechanism · catalyst · *in situ* electron microscopy

Understanding the growth mechanism of carbon nanotubes (CNTs) is of great importance for their efficient and controllable synthesis. Recently, notable progress has been made in controlling the purity,[1] growth position,[2] alignment,[3] length,[4] diameter,[5] and transport properties[6−8] of CNTs by catalytic chemical vapor deposition (CVD), where optimizing the size, position, composition, and pretreatment of catalysts plays a key role. In addition, CNTs with narrow chirality distributions have been synthesized by carefully tuning the composition of catalysts,[9−15] indicating the significance of catalyst-carbon interaction for the chirality control of CNTs. However, a thorough understanding of the nucleation and growth mechanism of CNTs is still urgently required for the precise control of their structure and properties.[16,17] It is generally considered that the growth of CNTs from traditional iron-group metal catalysts follows a vapor—liquid—solid (VLS) mechanism, where the catalytically decomposed carbon species are absorbed and dissolved into a catalyst nanoparticle (NP) to form a liquid-state carbide phase, and carbon is precipitated due to oversaturation to nucleate CNTs. However, such a growth mechanism is intensely debated, especially concerning the nature of the catalyst NPs.[18−24] Moreover, it has been discovered in recent years that noniron group metals, such as Au, Pt, Ag, Cu, *etc.*, can also be used to grow CNTs.[25−31] These metals have different physical and chemical properties, such as the binding energy with carbon, formation energy of carbides, catalytic ability, and melting points.[32−34] Accordingly, new questions arose. Is there a universal growth mechanism for all the metal catalysts? What is the nature of these diversified catalysts during the nucleation of CNTs? To answer these questions, a comparative investigation of the nucleation and growth process of CNTs

* Address correspondence to cliu@imr.ac.cn, golberg.dmitri@nims.go.jp.

Received for review July 29, 2013 and accepted December 19, 2013.

Published online December 19, 2013
10.1021/nn403927y

from different types of catalysts is highly desired to understand their growth mechanisms.

Among various investigation techniques, *in situ* transmission electron microscopy (TEM) has the advantage of providing direct, real time and high resolution characterizations of the materials and processes. The growth of CNTs from Fe-group metals has been observed in an environmental TEM, providing insight into the structure of the catalyst, carbon precipitation position, and carbon cap nucleation process.[18,20−22,35−37] While this approach can mimic the gas phase and high temperature environment for the CNT growth, it is necessary to modify the TEM chamber or use designated *in situ* cells to truly replicate the process. Recently, an alternative approach was developed, where electron beam irradiation and *in situ* heating were combined to investigate the interaction of carbon and metal catalyst NPs,[38−41] as well as the catalyst-free formation of CNTs.[42,43] However, the catalysts investigated are usually limited to iron-group metals, which are encapsulated in the hollow CNT channels during the CVD growth process.

Here we report a simple and versatile *in situ* TEM approach that is capable of studying the growth mechanism of CNTs from a variety of catalysts (Figure 1). The basic idea is to use a NP-loaded CNT as a nanosize furnace for the growth of CNTs with the aid of Joule heating and electron irradiation. First, CNTs with controllable diameter and length and two open ends were prepared by an anodic aluminum oxide (AAO) template method.[44] These CNTs are poorly crystallized, and are about tens of nanometers in diameter, having lengths around several micrometers. They are denoted as "AAO-CNTs" in this work. Then catalyst NPs were loaded inside the hollow core of the AAO-CNTs with good selectivity and controllability of their composition and dimensions.[45] A catalyst NP-loaded CNT was selected and biased to generate current with the aid of a TEM-STM holder inside a TEM chamber (Figure 1a,b). The Joule heating provides temperature and power for CNT growth, and electron beam irradiation-induced carbon injection provides active carbon species (Figure 1c). Finally, CNTs were grown from the catalyst NPs loaded inside the AAO-CNT nanofurnace (Figure 1d). The nucleation and growth process of the CNTs and the interaction between catalyst NPs and CNTs were studied *in situ* with atomic resolution. In the present work, this technique was used to study the nucleation and growth of CNTs from a traditional iron oxide catalyst and an Au catalyst.

RESULTS AND DISCUSSION

First, the roles of Joule heating and electron irradiation in our experiments are investigated. The temperature distribution of the AAO-CNT nanofurnace under biasing was simulated by finite element modeling (COMSOL Multiphysics 4.3b). As shown in Figure S1a (Supporting Information), a model was built by clamping a CNT between two Au electrodes. The inner

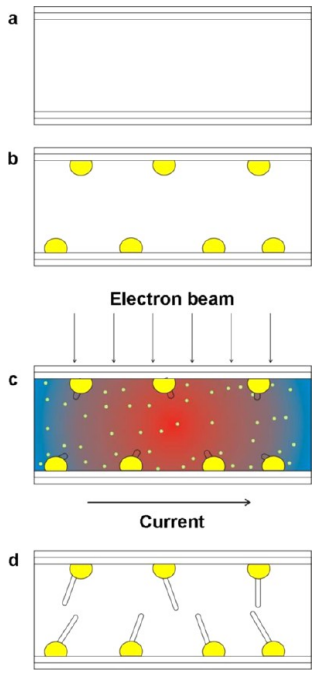

Figure 1. Schematic showing the experimental procedures of the *in situ* TEM method for investigating the growth mechanism of CNTs. (a) A CNT "nanofurnace" with two open ends prepared by the AAO template method. (b) Loading of catalyst NPs inside the hollow core of the AAO-CNT "nanofurnace". (c,d) *In situ* observation of CNTs nucleation driven by Joule heating and carbon atoms injection by electron beam irradiation.

diameter, outer diameter, and length of the CNT are 15, 25, and 300 nm, respectively. The Au electrodes have a cone shape similar to the STM tips used in our *in situ* probing experiments. When the bias was applied, heat was generated due to Joule heating effect. As can be seen in Figure S1b (Supporting Information), the middle part of the CNT turns to be "hot spot", while the Au electrodes remain roughly room temperature. The temperature distribution along the CNT is plotted in Figure S1c (Supporting Information), which follows a parabolic distribution, with the highest temperatures at around 1330 and 1080 K under a bias of 1.4 and 1.3 V, respectively. Therefore, under typical biasing condition in our experiments, the nanoparticles inside the nanofurnace could reach to the quasi-melting temperature, which is suitable for the growth of CNTs.

The effect of electron irradiation is investigated by applying a convergent electron beam onto an Au-NP filled CNT (Figure S2, and Movie S1, Supporting Information). It is commonly known that when no bias is applied, the CNT will become disordered and quickly damaged within a few minutes due to the knock-on effects. The high voltage (300 kV) is higher than the displacement threshold of carbon (~80 kV), and carbon atoms could be displaced easily. While under biasing of ~1.0 V and a current of ~22 μA, the CNT was observed to shrink gradually due to loss of carbon atoms, with its diameter reducing from 44.1 to 35.4 nm

(Figure S2a–c, Supporting Information) in about 16 min. In the meantime, ordered carbon shells are observed to be grown on the surface of the Au NP (Figure S2d). These results indicate that electron irradiation results in the injection of carbon atoms, which is consistent with previous reports.[38,39]

The state and structural changes of the iron oxide catalyst during the nucleation of CNTs were investigated. It was reported that the pretreatment history of catalyst NPs has an important influence on the growth efficiency[1] and chirality distribution of the grown CNTs.[7,46] Most of previous *in situ* TEM studies dealt with elemental iron-group metals.[18,20,21,35–39] However, in the catalytic CVD growth process, the catalysts are usually prepared by chemical methods or subjected to activation by heating in air, leading to the formation of metal oxides.[47–50] In this study, to fully reveal the structural changes in such catalysts, Fe_2O_3 NPs were used as the starting material (Figure S3, Supporting Information). CNTs with two open ends were prepared by an AAO template method.[51] These CNTs have a uniform diameter and length of ~50 nm and ~10 μm (Figure 2a), respectively. They are poorly crystallized because of the low carbon deposition temperature (~650 °C), which is typified by curved graphitic structures and homogeneous disordered contrast in the central area (Figure 2b). For catalyst NP loading, the CNTs were immersed in an ethanol solution of $Fe(NO_3)_3$. After heat treatment, Fe_2O_3-loaded CNTs were obtained. As shown by the HRTEM image and fast Fourier transform (FFT) pattern in Figure 2c,d, the loaded Fe_2O_3 NPs are highly crystalline and about 5–10 nm in diameter.

Fe_2O_3 NP-loaded CNTs were placed on an *in situ* TEM-STM holder (Nanofactory Instruments AB), through which a tunable bias was applied to generate a current. The temperature of the CNT nanofurnace was gradually increased by increasing the current. TEM images and corresponding FFT patterns of the original Fe_2O_3 NPs and the structure changes during the heating process are shown in Figure S4 (Supporting Information). Initially, the Fe_2O_3 NPs have a diameter of 5–10 nm, are highly crystalline, and give sharp diffraction spots (Figure S4a,b, Supporting Information). When a direct current of 36 μA was passed, while the shape of the NPs remained unchanged (Figure S4c,d, Supporting Information), the Fe_2O_3 NPs started to react with the surrounding carbon to form Fe_3C, as indicated by the appearance of Fe_3C (201) diffraction spots and the disappearance of some Fe_2O_3 (311) diffraction spots in the FFT pattern (Figure S4d, Supporting Information). When the current reached 40 μA, small Fe_3C NPs merged to form large Fe_3C particles with a diameter of ~15 nm (Figure S4e, Supporting Information). Accordingly, the diffraction spots of Fe_2O_3 disappear completely, and only the diffraction pattern of Fe_3C can be observed (Figure S4f, Supporting Information).

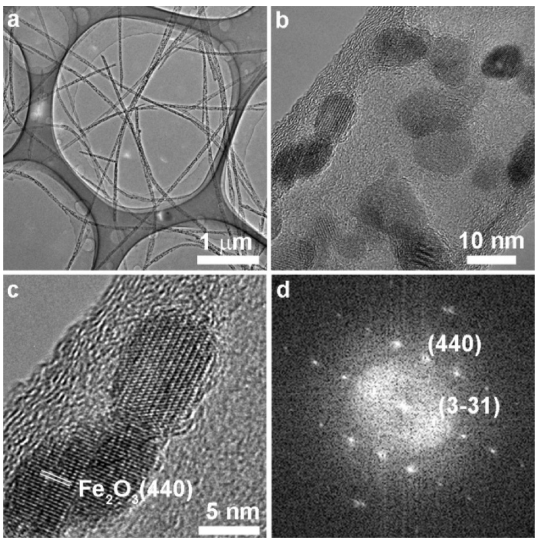

Figure 2. TEM characterizations of Fe_2O_3 NP-loaded AAO-CNTs. (a,b) TEM images showing the uniform structure of the AAO-CNTs and loaded Fe_2O_3 NPs, (c,d) HRTEM image and FFT pattern demonstrating that the Fe_2O_3 NPs are single-crystalline with a diameter from 5 to 10 nm, and the AAO-CNTs are poorly crystalline with curved and discontinuous contrast.

Subsequently, the Fe_3C NPs started to move with their shape frequently changing, indicating that they are in a liquid-like state (Figure 3a and Movie S2, Supporting Information). In the meantime, amorphous carbon at the lower left part of the NP (indicated by a white arrow) began to dissolve into the NP, and graphitic shells were found to precipitate from the upper right part of the NP, as indicated by a black arrow in Figure 3a. It is interesting to note that the precipitation of the graphitic shell is not symmetric around the NP, which was previously reported for a Ni-catalyzed growth of CNTs under environmental TEM.[18,20,52] This can be attributed to the preferred precipitation of carbon at the stepped Fe_3C–C interface, which extended around the catalyst NP. Along with the precipitation of the graphitic shell, the NP was elongated along the graphitic shell. At the same time, part of the NP congregated to the lower right direction (Figure 3b), and graphitic shells started to precipitate from the upper left side of the NP (Figure 3c), which is opposite to the carbon precipitation direction. The fact that the carbon dissolution and precipitation occurs at diametrically opposite sites indicates that carbon is transferred through the NP by bulk diffusion. Such a phenomenon can be explained from the phase diagram. The liquidus temperature depends on the concentration of carbon. The dissolution or precipitation of carbon will lower or raise the liquidus temperature, respectively, and therefore enhances or depresses the deformability and fluidity of different parts of the catalyst NPs. During these processes, crystalline lattices with strain contrast could be seen in part of the NP (Figure 3c), but the remainder of the NP was found to be liquid with a homogeneous contrast. Therefore, the catalyst was confirmed to be in a partially

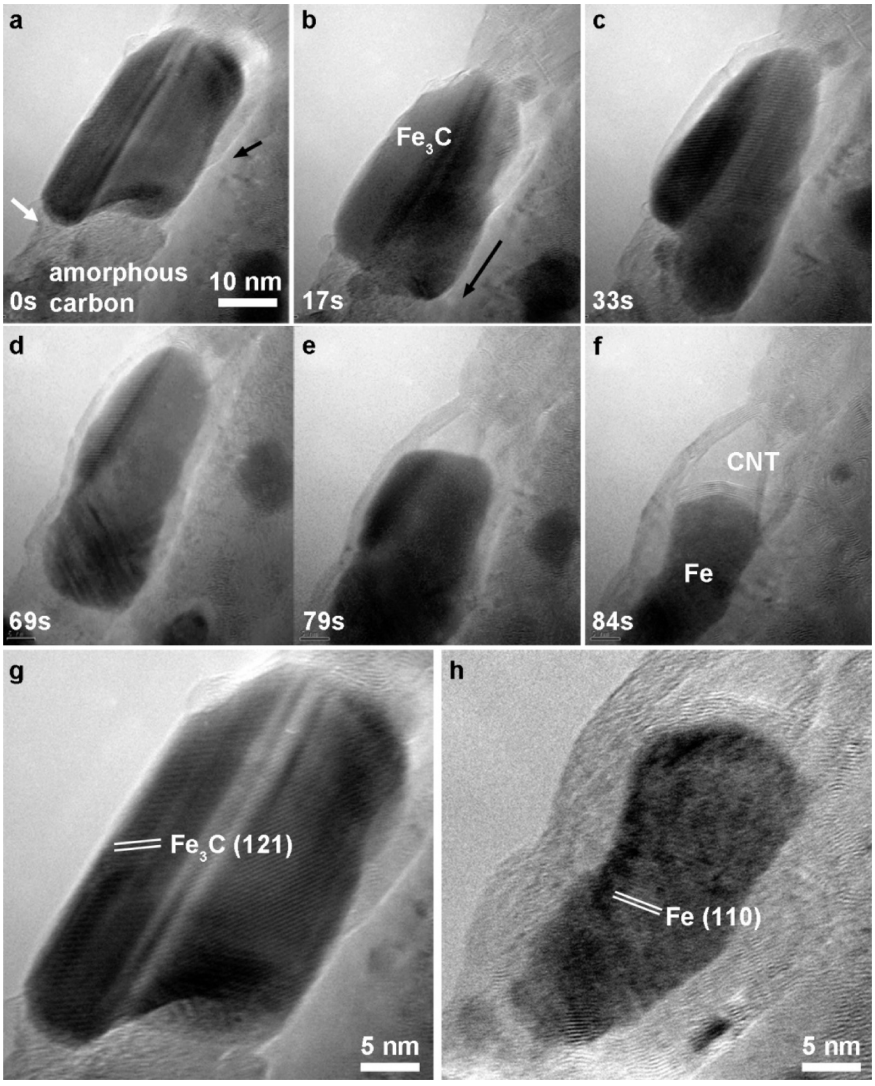

Figure 3. *In situ* **TEM observations of the nucleation and growth of a CNT from an iron oxide catalyst NP. (a–c) Shape fluctuations of the catalyst NP and dissolution of amorphous carbon, and precipitation of a graphitic shell at the edge of the catalyst NP. (d,e) Movement of the catalyst NP and the growth of a CNT. (f) Cessation of the CNT growth. (g) HRTEM image of the NP during CNT growth, showing its crystalline Fe_3C structure. (h) HRTEM image of the NP after CNT growth, showing that the encapsulated NP is elemental Fe.**

liquid state. After another 36 s, the surface of the NP was covered by graphitic shells except for the lower part (Figure 3d). The NP was expelled to the lower position, leaving a hollow space (Figure 3e), and thus a CNT was formed. Growth ended when the graphitic shells had completely encapsulated the whole catalyst NP, indicating that the driving force of the nucleation and growth of CNTs is the chemical potential difference between the disordered carbon and highly crystalline graphitic shells. Along with the growth cessation, the volume of the catalyst NP was decreased and surrounded by a graphitic shell (Figure 3f). HRTEM images of the catalyst NP during and after CNT growth are shown in Figure 3g and 3h, respectively. Lattices corresponding to a Fe_3C (121) plane could be identified in the catalyst NP during the CNT growth (Figure 3g), while the NP was transformed into a body-centered cubic (BCC) Fe phase when the growth ended (Figure 3h).

Fe-group metals and alloys are the most commonly used catalysts for the growth of CNTs. It is generally accepted that CNTs grow from these metal catalysts following a VLS mechanism by bulk diffusion through a liquid carbide phase.[53,54] However, controversial results have been reported about the composition, phase, and physical state of the active catalyst. For example, it was reported by many groups that Fe, Co, Ni and their alloy catalysts exist in a metallic state rather than as a carbide phase during CNT nucleation and growth,[11,12,18,20,22,23,55] while Yoshida *et al.* and Nishimura *et al.* reported that the active phase of iron catalysts is iron carbide on the basis of *in situ* TEM and X-ray diffraction analysis.[19,21] Through our *in situ* TEM observations on the structural evolution of the Fe_2O_3 catalyst NP, it was revealed that the catalyst NP is in different states during different stages. During the nucleation and growth of CNTs, the catalyst is in a

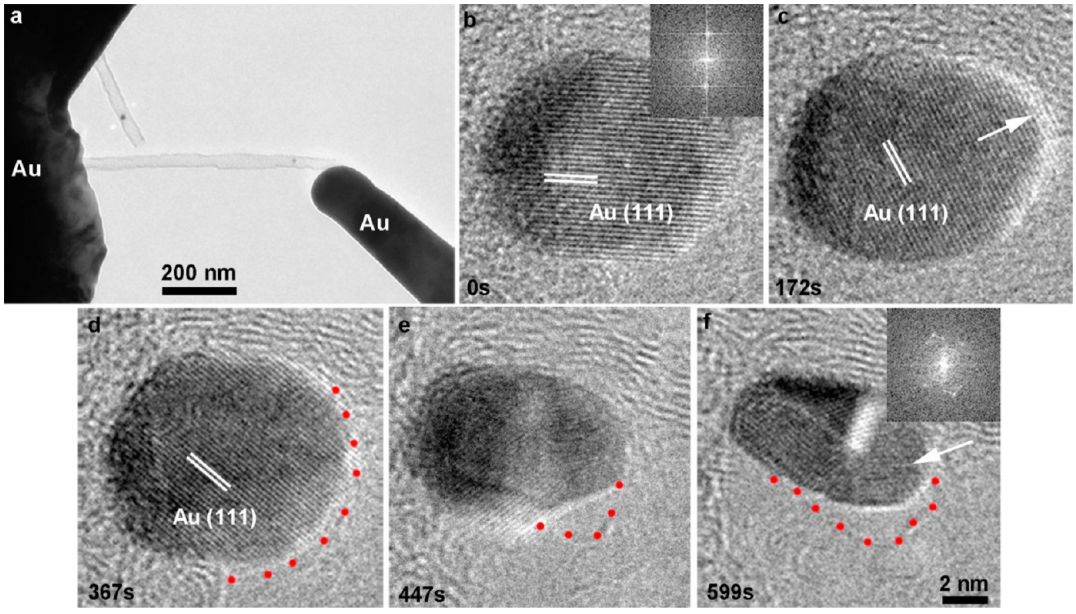

Figure 4. *In situ* **TEM observations of the nucleation of a CNT from an Au catalyst NP. (a) TEM image of the experimental configuration. An Au NP-loaded AAO-CNT "nanofurnace" was connected between two gold electrodes. (b) Initial Au NP with single-crystalline structure, as shown by the Au (111) lattice fringes and the FFT pattern. (c) Fluctuation of the Au NP under Joule heating, both in the crystalline orientation and dimension. (d) Formation of a continuous graphitic shell on the surface of the fluctuating Au NP. (e,f) A carbon cap is formed by partial detachment from the downsized Au NP.**

carbide phase and the NP is transformed into metallic Fe after the growth ceased. Moreover, in contrast to the traditional VLS mechanism involving a single liquid phase, different physical states such as a liquid-like state with fast diffusivity but also long-range crystalline order[18,20] and a fluctuating solid state[21] have been reported. In our work, a partially liquid state, which is caused by the dynamic processes of carbon dissolution and precipitation, was observed. From the above discussion, we can see that the traditional VLS mechanism is oversimplified when describing the state of the catalyst NPs during the growth of CNTs. The Fe catalyst NPs could be in elemental metal or carbide phase at different growth stages. And the physical states of the catalyst, such as solid, liquid, or partial liquid, depend on the local kinetic conditions.

The state and structural changes of Au NPs during CNT nucleation were investigated using the same approach as described above (Movie S3, Supporting Information). Single-crystalline Au NPs with diameters of 5−10 nm were placed inside the hollow core of AAO-CNTs (Figure S5, Supporting Information). As shown in Figure 4a, an Au NP-loaded AAO-CNT was loaded in the *in situ* TEM-STM holder and connected between two gold electrodes. The diameter of the spherical Au NP is about 9.5 nm, and the NP is a single crystal as demonstrated by Au (111) lattices (Figure 4b) and also by the sharp diffraction spots in the FFT pattern (inset of Figure 4b). The Au NP is surrounded by amorphous carbon as shown by the curved and noncontinuous contrast. The AAO-CNT nanofurnace was then heated by passing a current through it. The Au NP changed into a fluctuating state (Figure 4c,d), and Au (111) lattice fringes were observed to change directions indicating the fluctuating crystalline orientations. In the meantime, the dimension of the Au NP was also fluctuating from near spherical to an elongated shape as marked by the arrow in Figure 4c. Such frequent fluctuations suggest that the Au NP has been in a quasi-melting state.[56,57] No chemical reaction between Au and carbon was observed, as shown by the uniform Au (111) lattices inside the whole Au NP. The chemical inertness of the Au NP is in contrast to the chemically active Fe catalyst NPs. Under further heating, a continuous graphitic shell was formed on the surface of the Au NP as marked by red dots in Figure 4d. The graphitic shell was closely attached to the surface until the Au NP was downsized to an ellipsoidal shape with a length and width around 9.2 and 6.5 nm, respectively, probably due to partial vaporization or thermally assisted diffusion (Figure 4e,f). The smaller Au NP became more active with faster changes. In addition, the resolved crystalline lattices and the inserted FFT pattern show that the Au NP became polycrystalline (Figure 4f). During the downsizing, the graphitic shell wrapping the Au NP also became smaller. As a result, the circumference of the graphitic shell was reduced from 33.4 to 26.6 nm. However, because of rapidly fluctuating Au NP, a segment of the graphitic shell (a carbon "cap") was found to be detached from the Au NP as indicated by the red dots in Figure 4e,f. Meanwhile, the base of the cap was still tightly attached to the edge of the Au NP. Therefore, the critical step of the nucleation of a CNT, that is, the formation of a carbon cap attached to a catalyst NP, was

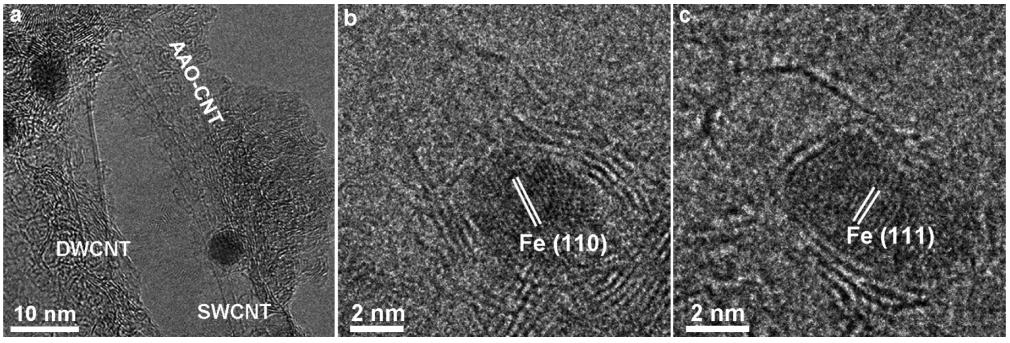

Figure 5. *Ex situ* **growth of CNTs by CVD using the Fe_2O_3 NPs-filled AAO-CNT as catalyst. (a) TEM image of the as-grown single-wall and double-wall CNTs inside the AAO-CNT. (b,c) HRTEM images of the short CNTs at the nucleation stage. The catalyst-NPs after growth are metallic Fe phase, encapsulated in a complete graphitic shell.**

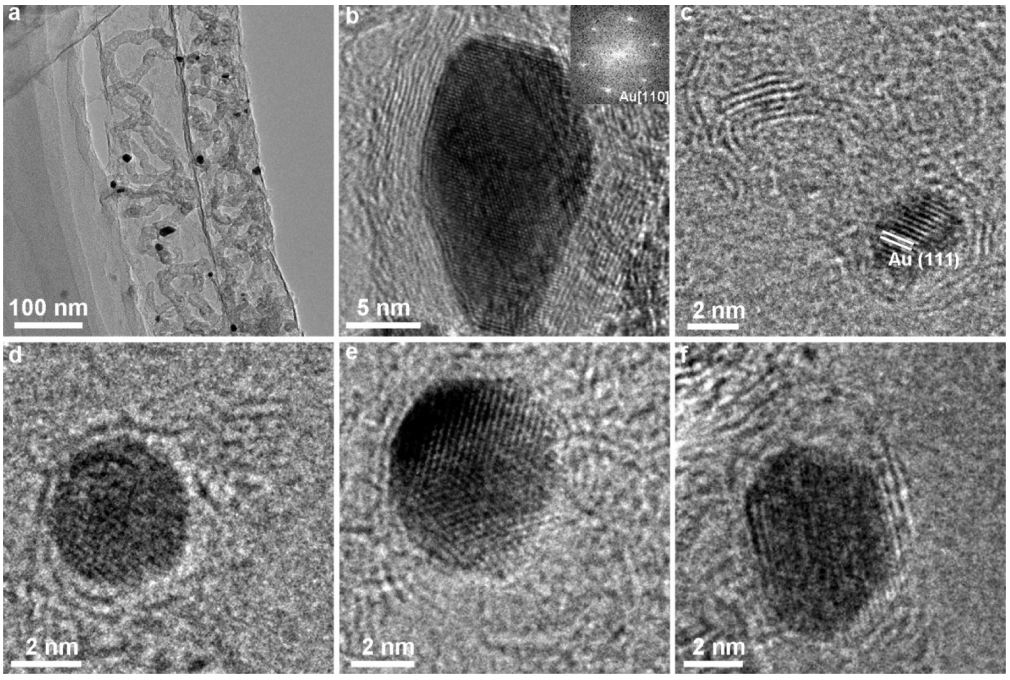

Figure 6. *Ex situ* **growth of CNTs by CVD using the Au NPs-filled AAO-CNT as catalyst. (a) Low-mag TEM image showing the grown CNTs inside the hollow core of AAO-CNTs. (b) HRTEM image of a CNT grown from a single crystalline Au NP. (c–f) HRTEM images showing short CNTs at the nucleation stage attached to Au NPs. For these active Au NPs, carbon shells are partially coated on the surface forming protruded and lifted carbon caps.**

completed. The fact that the carbon cap became smaller than the one initially wrapping the Au NP suggests that some of the carbon may be dissolved into the Au NP. From the equilibrium Au–C phase diagram, carbon has a solubility of 4.7 at % in liquid phase of gold.[58] And it was reported that the solubility could be increased because of the nanometer size of the NPs.[59] In our experiment, when the carbon cap was formed (Figure 4f), the Au NP showed disordered contrast in the region close to the carbon cap as marked by the arrow, which could be caused by the dissolution of carbon. While no chemical reaction between Au and carbon was observed, it is possible that some inhomogeneous cluster-like structures were formed locally because of the dissolution of carbon in the Au NPs. The structural features of the Au NPs, such as reorientation, size reduction, and size dependent interactions with carbon are consistent with previous *ex situ* reports of CNT growth from gold and copper.[25–27,60,61] It was reported that the formation of carbide phases is not energetically favored for gold, which can explain why Au remained metallic rather than forming a carbide during the nucleation of the carbon caps. In addition, the binding energy of gold with carbon is much smaller than that of Fe-group metals,[60,62] which could be the reason for the partial detachment of the graphitic shell from the fluctuating Au NP surface.

Besides the *in situ* TEM observations on the nucleation of CNTs, *ex situ* parallel experiments were also carried out to grow CNTs using the Fe_2O_3 and Au NPs-loaded AAO-CNTs as catalyst (Scheme S1, Supporting Information). Abundant CNTs were grown from both of the catalysts (Figure 5 and Figure 6), suggesting that

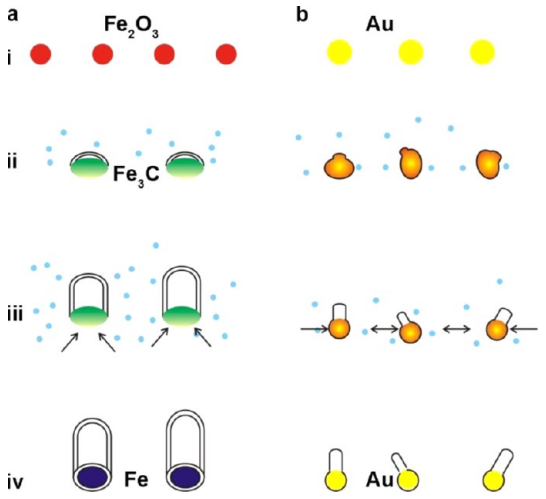

Figure 7. Schematic of the proposed growth models for the growth of CNTs from (a) Fe_2O_3 and (b) Au NPs. The Fe catalyst NP undergoes a series of structural changes, including: (i,ii) reduction of Fe_2O_3 to Fe_3C, carbon dissolution and precipitation from the partially liquid and fluctuating Fe_3C NP; (iii) movement of the Fe_3C NP due to its expulsion from the precipitated graphitic shells; and (iv) formation of elemental Fe after CNT growth stops. For the Au NP: (i,ii) assembly of a graphitic shell on the fluctuating Au NP; (iii) partial detachment of the graphitic shell during the fluctuations and formation of a carbon cap; (iv) continued growth of a CNT from the protruding carbon cap.

the NPs in our *in situ* experiments are also effective in normal CVD growth process. For the Fe_2O_3 NPs, high quality single-walled and double-walled CNTs were observed grown inside the channels of the AAO-CNTs (Figure 5a). The nanotube shown in Figure 5b has a length and a diameter of 10.7 and 5.2 nm, respectively. The catalyst NP can be identified as BCC-Fe, as revealed by the Fe (110) lattices. And the CNT in Figure 5c is around 9.4 nm in length and 3.9 nm in diameter, and the catalyst NP is face-centered cubic (FCC)-Fe, with the Fe (111) lattices resolved. Importantly, both the catalyst NPs are surrounded by closed graphitic shells, indicating that carbon was precipitated from the NPs when the growth ceased. This is consistent with the *in situ* TEM observations that the active catalyst phase is Fe_3C and it is transformed into elemental Fe after the growth is ceased.

Figure 6 shows the products obtained by CVD growth using the Au NPs-filled AAO-CNTs as catalyst. It can be seen that many CNTs are formed inside the hollow cores of the AAO-CNTs. Distinct from the straight single-wall and double-wall nanotubes grown from the Fe_2O_3 NPs, most of the nanotubes from the Au NPs are multiwalled, highly curved, and bamboo-structured (Figure 6a). This is possibly because that the catalytic activity of the Au NPs is lower than that of the Fe_2O_3 NPs. HRTEM image of the catalyst (Figure 6b) reveals that the NP is single crystalline Au with [110] zone axis and the local structure of the nanotube is graphitized. In addition, HRTEM images were taken for the Au NPs at the stage of CNT nucleation (Figure 6c–f). For these active Au NPs, carbon shells are partially coated on the surfaces, with the protrusion (Figure 6d) and lift-up of carbon caps observed (Figure 6e,f). These *ex situ* after-growth observations are consistent with the *in situ* TEM results that the Au NPs could promote the graphitization of carbon structures. And the various shapes from sphere (Figure 6d) and ellipsoid (Figure 6e) to elongated polyhedrons (Figure 6b,f) are consistent with the *in situ* TEM observations that the Au NPs are fluctuating during the nucleation of CNTs.

The distinctly different behaviors of Fe and Au catalyst NPs during the nucleation and growth of CNTs are summarized in Figure 7. For the Fe_2O_3 NPs: (i) the catalyst NPs are reduced to Fe_3C; (ii) during the growth of CNT, graphitic shells precipitate from a partially liquid Fe_3C NP; (iii) Fe_3C NP is expelled by the precipitated graphitic shells, leaving a hollow channel; (iv) when the CNT growth ceases, the carbon dissolved in the NP completely precipitates to form a closed graphitic shell, and the surrounded NP is transformed to the metallic Fe phase. For the Au NPs: (i,ii) carbon atoms assemble into a graphitic shell on the template of the Au NP, and the wrapping graphitic shell follows the fluctuating Au NP in both shape and size; (iii) the graphitic shell is partially detached from the Au NP during the fluctuations to form a carbon cap; (iv) under suitable conditions, the carbon cap grows into a CNT by continuously incorporating carbon atoms. In both processes, the active catalyst NPs are in a partially liquid state, with frequent fluctuations in shape, size, crystalline orientation, and physical states. The major difference is the chemical reaction routes. While the Fe catalyst NPs undergo a series of transitions from oxide to carbide and finally to the metallic state, no bulk chemical reactions or phase transitions occur for the Au catalyst NPs. Therefore, from our *in situ* TEM observations, a universal growth mechanism for metal-catalyzed CNT growth does not exist. However, it is the difference of the interaction between catalysts and carbon that enables the production of SWCNTs with a narrow distribution of chiralities.[9−14] Therefore, with continuing investigations on the specific interactions of carbon with different catalysts, the chirality-selective synthesis of CNTs could hopefully be realized by catalyst engineering.

CONCLUSIONS

A simple, versatile *in situ* TEM method has been developed for investigating the nucleation and growth mechanism of CNTs from various catalysts. The traditional iron oxide NP and recently emerging gold NP catalysts were studied as examples. It was revealed that the traditional vapor−liquid−solid mechanism is oversimplified in describing the growth of CNTs, and different catalysts may have distinct and changing physical states, chemical compositions and structures

at different stages of the CNT nucleation and growth process, owing to their differed physicochemical properties and kinetic conditions. Our *in situ* TEM comparative investigations and understanding on the growth process and mechanism of different catalysts may be helpful for the metallicity- and chirality-controlled synthesis of CNTs.

METHODS

Fabrication of CNT "Nanofurnaces" by the AAO Template Method and Loading of Catalyst NPs. The details of the preparation of CNTs with two open ends by the AAO template method were described in a previous paper.[45] In brief, AAO templates were produced by a two-step anodization at 40 V in an aqueous solution containing 3 wt % oxalic acid at 20 °C. Carbon was deposited in the channels of the AAO templates by CVD of C_2H_2 at 650 °C. The diameter and length of the CNTs were very uniform and could be easily controlled by tuning the fabrication parameters, such as the voltage, electrolyte concentration, and anodizing time. Next, catalyst NPs were placed in the hollow cores of the CNTs. For loading of Fe_2O_3 catalyst, AAO template-supported CNTs were immersed in an ethanol solution of $Fe(NO_3)_3$ and ultrasonicated at room temperature for 3 h; then the sample was heated to 400 °C under a N_2 flow and held for 3 h. Finally, the AAO templates were removed by immersing them in a 5 M NaOH aqueous solution, and free-standing iron oxide NP-loaded CNTs were obtained. For loading of Au catalyst, the AAO template-supported CNTs were immersed in an ethanol solution of $HAuCl_4$ and ultrasonicated at room temperature for 3 h; then the sample was heated to 200 °C under a H_2 flow and held for 3 h. After removing the AAO template by immersing it in a 5 M NaOH aqueous solution, free-standing gold NP-loaded CNTs were obtained.

Parallel *Ex Situ* Growth of CNTs in AAO-CNTs by CVD. The experimental procedure for the growth of CNTs inside the AAO-CNT is described in Scheme S1 (Supporting Information). The fabrication of AAO templates, deposition of carbon in AAO channels, and loading of catalysts were carried out similarly with the previous section (Scheme S1a–c, Supporting Information). Then CNTs were grown from the loaded Fe_2O_3 and Au NPs at 900 °C (Scheme S1d, Supporting Information). First, the furnace was heated up to the growth temperature under Ar flow of 250 mL/min. Pretreatment of Au NPs was done under H_2 flow of 500 mL/min for 15 min. Then a mixture of H_2/CH_4 flow of 60/60 mL/min was introduced for the CNTs growth. The growth lasted for 1 h, and then the furnace was cooled to room temperature under Ar flow. Lastly, the AAO template was removed in a 5 M NaOH aqueous solution.

***In Situ* TEM Observation of the States and Structural Changes of Catalysts during CNT Nucleation.** A catalyst NP-loaded CNT "nanofurnace" was manipulated with a TEM-STM holder (Nanofactory Instruments AB), which was then inserted into a TEM (Tecnai F20 or JEM-3100FEF). A direct current was passed through the isolated CNT "nanofurnace" to generate a suitable temperature for CNT growth by Joule heating. In the meantime, electron beam-induced carbon atom injection from the wall of the parent CNT could provide active carbon species. CNTs were thus nucleated and grown from the loaded catalyst NPs. A CCD camera (Gatan Ultrascan 894) was used for real time observations and video recording of the CNT growth process and catalyst structural changes.

Finite Element Modeling of the Temperature Distribution of the Nanofurnace. The governing equation is the heat equation in solid: $\rho C_p(\partial T/\partial t) - \nabla(k\nabla T) = Q$, where ρ is the density, C_p is the heat capacity, k is the thermal conductivity, and $Q = J \cdot E$ is the heat source from the Joule heating, where J and E are the current density and electric field, respectively. End surfaces of the gold electrode were treated as heat sink and kept at room temperature (293.15 K). Surface-to-ambient radiation was applied to all the surfaces: $q = \varepsilon\sigma AT^4$, where ε is the surface emissivity (assumed to be 0.9), σ is the Stefan–Boltzmann constant, and A is the surface area. To keep the essential physics, the dependence of the thermal conductance (k) and electrical resistivity (R) of the CNTs were neglected in our simulations. A moderate thermal conductance of 10 W/mK was adopted for the AAO-CNTs, considering that they were synthesized at a relatively low temperature (650 °C) and have rather disordered structure. The electrical conductivity of the CNT was measured by I–V testing to be around 1.85×10^4 S/m. Because of the tight contact between CNT and the electrodes, the contact thermal resistance was neglected in our simulations. Initially, the temperature was set to be at room temperature.

Conflict of Interest: The authors declare no competing financial interest.

Acknowledgment. Valuable discussions with Dr. Chenghua Sun, Dr. Li-Chang Yin, and Dr. Bilu Liu are acknowledged. We thank Dr. Oleg Lourie, Dr. Chuanbin Jiang, Mr. Bo Wu, Dr. Isamu Yamada, and Dr. Masanori Mitome for technical assistance. This work is supported by Ministry of Science and Technology of China (Grant 2011CB932601), National Natural Science Foundation of China (Grants 51221264, 51272257, 51102242), and JSPS KAKENHI Grant Number 25820336, International Center for Young Scientists (ICYS), World Premier International (WPI) Center for Materials Nanoarchitectonics (MANA) of the National Institute for Materials Science (NIMS), Tsukuba, Japan.

Supporting Information Available: *In situ* TEM videos of the nucleation of CNTs from Fe_2O_3 and Au catalysts. Simulated temperature distribution in the AAO-CNT "nanofurnace". *In situ* TEM images of injection and deposition of carbon atoms by electron beam. EDX spectrum of the Fe_2O_3 NPs-loaded CNTs. Structural changes of a Fe_2O_3 NP-loaded CNT under Joule heating. Characterization of Au NP-loaded CNTs. *Ex situ* growth process of CNTs in AAO-CNTs. This material is available free of charge *via* the Internet at http://pubs.acs.org.

REFERENCES AND NOTES

1. Hata, K.; Futaba, D. N.; Mizuno, K.; Namai, T.; Yumura, M.; Iijima, S. Water-Assisted Highly Efficient Synthesis of Impurity-Free Single-Walled Carbon Nanotubes. *Science* **2004**, *306*, 1362–1364.
2. Kong, J.; Soh, H. T.; Cassell, A. M.; Quate, C. F.; Dai, H. Synthesis of Individual Single-Walled Carbon Nanotubes on Patterned Silicon Wafers. *Nature* **1998**, *395*, 878–881.
3. Zhang, Y. G.; Chang, A. L.; Cao, J.; Wang, Q.; Kim, W.; Li, Y. M.; Morris, N.; Yenilmez, E.; Kong, J.; Dai, H. J. Electric-Field-Directed Growth of Aligned Single-Walled Carbon Nanotubes. *Appl. Phys. Lett.* **2001**, *79*, 3155–3157.
4. Wen, Q.; Zhang, R. F.; Qian, W. Z.; Wang, Y. R.; Tan, P. H.; Nie, J. Q.; Wei, F. Growing 20 cm Long DWNTs/TWNTs at a Rapid Growth Rate of 80–90 mu m/s. *Chem. Mater.* **2010**, *22*, 1294–1296.
5. Cheung, C. L.; Kurtz, A.; Park, H.; Lieber, C. M. Diameter-Controlled Synthesis of Carbon Nanotubes. *J. Phys. Chem. B* **2002**, *106*, 2429–2433.
6. Kim, W.; Choi, H. C.; Shim, M.; Li, Y.; Wang, D.; Dai, H. Synthesis of Ultralong and High Percentage of Semiconducting Single-Walled Carbon Nanotubes. *Nano Lett.* **2002**, *2*, 703–708.
7. Harutyunyan, A. R.; Chen, G.; Paronyan, T. M.; Pigos, E. M.; Kuznetsov, O. A.; Hewaparakrama, K.; Kim, S. M.; Zakharov, D.; Stach, E. A.; Sumanasekera, G. U. Preferential Growth of Single-Walled Carbon Nanotubes with Metallic Conductivity. *Science* **2009**, *326*, 116–120.
8. Hong, G.; Zhang, B.; Peng, B. H.; Zhang, J.; Choi, W. M.; Choi, J. Y.; Kim, J. M.; Liu, Z. F. Direct Growth of Semiconducting Single-Walled Carbon Nanotube Array. *J. Am. Chem. Soc.* **2009**, *131*, 14642.
9. Bachilo, S. M.; Balzano, L.; Herrera, J. E.; Pompeo, F.; Resasco, D. E.; Weisman, R. B. Narrow (n,m)-Distribution

of Single-Walled Carbon Nanotubes Grown Using a Solid Supported Catalyst. *J. Am. Chem. Soc.* **2003**, *125*, 11186–11187.
10. Li, X.; Tu, X.; Zaric, S.; Welsher, K.; Seo, W. S.; Zhao, W.; Dai, H. Selective Synthesis Combined with Chemical Separation of Single-Walled Carbon Nanotubes for Chirality Selection. *J. Am. Chem. Soc.* **2007**, *129*, 15770–15771.
11. Chiang, W.-H.; Mohan Sankaran, R. Linking Catalyst Composition to Chirality Distributions of as-Grown Single-Walled Carbon Nanotubes by Tuning Ni_xFe_{1-x} Nanoparticles. *Nat. Mater.* **2009**, *8*, 882–886.
12. Chiang, W.-H.; Sakr, M.; Gao, X. P. A.; Sankaran, R. M. Nanoengineering Ni_xFe_{1-x} Catalysts for Gas-Phase, Selective Synthesis of Semiconducting Single-Walled Carbon Nanotubes. *ACS Nano* **2009**, *3*, 4023–4032.
13. He, M.; Chernov, A. I.; Fedotov, P. V.; Obraztsova, E. D.; Sainio, J.; Rikkinen, E.; Jiang, H.; Zhu, Z.; Tian, Y.; Kauppinen, E. I.; *et al.* Predominant (6,5) Single-Walled Carbon Nanotube Growth on a Copper-Promoted Iron Catalyst. *J. Am. Chem. Soc.* **2010**, *132*, 13994–13996.
14. Wang, H.; Wang, B.; Quek, X.-Y.; Wei, L.; Zhao, J.; Li, L.-J.; Chan-Park, M. B.; Yang, Y.; Chen, Y. Selective Synthesis of (9,8) Single Walled Carbon Nanotubes on Cobalt Incorporated TUD-1 Catalysts. *J. Am. Chem. Soc.* **2010**, *132*, 16747–16749.
15. Liu, B.; Ren, W.; Li, S.; Liu, C.; Cheng, H.-M. High Temperature Selective Growth of Single-Walled Carbon Nanotubes with a Narrow Chirality Distribution from a CoPt Bimetallic Catalyst. *Chem. Commun. (Cambridge, U. K.)* **2012**, *48*, 2409–2411.
16. Jourdain, V.; Bichara, C. Current Understanding of the Growth of Carbon Nanotubes in Catalytic Chemical Vapour Deposition. *Carbon* **2013**, *58*, 2–39.
17. Liu, C.; Cheng, H.-M. Carbon Nanotubes: Controlled Growth and Application. *Mater. Today* **2013**, *16*, 19–28.
18. Helveg, S.; López-Cartes, C.; Sehested, J.; Hansen, P. L.; Clausen, B. S.; Rostrup-Nielsen, J. R.; Abild-Pedersen, F.; Nørskov, J. K. Atomic-Scale Imaging of Carbon Nanofibre Growth. *Nature* **2004**, *427*, 426–429.
19. Nishimura, K.; Okazaki, N.; Pan, L. J.; Nakayama, Y. *In Situ* Study of Iron Catalysts for Carbon Nanotube Growth Using X-Ray Diffraction Analysis. *Jpn. J. Appl. Phys., Part 2* **2004**, *43*, L471–L474.
20. Hofmann, S.; Sharma, R.; Ducati, C.; Du, G.; Mattevi, C.; Cepek, C.; Cantoro, M.; Pisana, S.; Parvez, A.; Cervantes-Sodi, F.; *et al. In Situ* Observations of Catalyst Dynamics during Surface-Bound Carbon Nanotube Nucleation. *Nano Lett.* **2007**, *7*, 602–608.
21. Yoshida, H.; Takeda, S.; Uchiyama, T.; Kohno, H.; Homma, Y. Atomic-Scale *In-Situ* Observation of Carbon Nanotube Growth from Solid State Iron Carbide Nanoparticles. *Nano Lett.* **2008**, *8*, 2082–2086.
22. Hofmann, S.; Blume, R.; Wirth, C. T.; Cantoro, M.; Sharma, R.; Ducati, C.; Havecker, M.; Zafeiratos, S.; Schnoerch, P.; Oestereich, A.; *et al.* State of Transition Metal Catalysts during Carbon Nanotube Growth. *J. Phys. Chem. C* **2009**, *113*, 1648–1656.
23. Wirth, C. T.; Hofmann, S.; Robertson, J. State of the Catalyst during Carbon Nanotube Growth. *Diamond Relat. Mater.* **2009**, *18*, 940–945.
24. Wirth, C. T.; Bayer, B. C.; Gamalski, A. D.; Esconjauregui, S.; Weatherup, R. S.; Ducati, C.; Baehtz, C.; Robertson, J.; Hofmann, S. The Phase of Iron Catalyst Nanoparticles during Carbon Nanotube Growth. *Chem. Mater.* **2012**, *24*, 4633–4640.
25. Zhou, W.; Han, Z.; Wang, J.; Zhang, Y.; Jin, Z.; Sun, X.; Zhang, Y.; Yan, C.; Li, Y. Copper Catalyzing Growth of Single-Walled Carbon Nanotubes on Substrates. *Nano Lett.* **2006**, *6*, 2987–2990.
26. Bhaviripudi, S.; Mile, E.; Steiner, S. A.; Zare, A. T.; Dresselhaus, M. S.; Belcher, A. M.; Kong, J. CVD Synthesis of Single-Walled Carbon Nanotubes from Gold Nanoparticle Catalysts. *J. Am. Chem. Soc.* **2007**, *129*, 1516–1517.
27. Yuan, D.; Ding, L.; Chu, H.; Feng, Y.; McNicholas, T. P.; Liu, J. Horizontally Aligned Single-Walled Carbon Nanotube on Quartz from a Large Variety of Metal Catalysts. *Nano Lett.* **2008**, *8*, 2576–2579.
28. Ghorannevis, Z.; Kato, T.; Kaneko, T.; Hatakeyama, R. Narrow-Chirality Distributed Single-Walled Carbon Nanotube Growth from Nonmagnetic Catalyst. *J. Am. Chem. Soc.* **2010**, *132*, 9570–9572.
29. Takagi, D.; Hibino, H.; Suzuki, S.; Kobayashi, Y.; Homma, Y. Carbon Nanotube Growth from Semiconductor Nanoparticles. *Nano Lett.* **2007**, *7*, 2272–2275.
30. Huang, S.; Cai, Q.; Chen, J.; Qian, Y.; Zhang, L. Metal-Catalyst-Free Growth of Single-Walled Carbon Nanotubes on Substrates. *J. Am. Chem. Soc.* **2009**, *131*, 2094–2095.
31. Liu, B.; Ren, W.; Gao, L.; Li, S.; Pei, S.; Liu, C.; Jiang, C.; Cheng, H.-M. Metal-Catalyst-Free Growth of Single-Walled Carbon Nanotubes. *J. Am. Chem. Soc.* **2009**, *131*, 2082–2083.
32. Raty, J.-Y.; Gygi, F.; Galli, G. Growth of Carbon Nanotubes on Metal Nanoparticles: A Microscopic Mechanism from *Ab Initio* Molecular Dynamics Simulations. *Phys. Rev. Lett.* **2005**, *95*, 096103.
33. Hamilton, J. C.; Blakely, J. M. Carbon Segregation to Single Crystal Surfaces of Pt, Pd and Co. *Surf. Sci.* **1980**, *91*, 199–217.
34. Haruta, M.; Yamada, N.; Kobayashi, T.; Iijima, S. Gold Catalysts Prepared by Coprecipitation for Low-Temperature Oxidation of Hydrogen and of Carbon Monoxide. *J. Catal.* **1989**, *115*, 301–309.
35. Sharma, R.; Iqbal, Z. *In Situ* Observations of Carbon Nanotube Formation Using Environmental Transmission Electron Microscopy. *Appl. Phys. Lett.* **2004**, *84*, 990–992.
36. Lin, M.; Tan, J. P. Y.; Boothroyd, C.; Loh, K. P.; Tok, E. S.; Foo, Y. L. Direct Observation of Single-Walled Carbon Nanotube Growth at the Atomistic Scale. *Nano Lett.* **2006**, *6*, 449–452.
37. Sharma, R.; Rez, P.; Treacy, M. M. J.; Stuart, S. J. *In Situ* Observation of the Growth Mechanisms of Carbon Nanotubes under Diverse Reaction Conditions. *J. Electron Microsc.* **2005**, *54*, 231–237.
38. Rodríguez-Manzo, J. A.; Janowska, I.; Pham-Huu, C.; Tolvanen, A.; Krasheninnikov, A. V.; Nordlund, K.; Banhart, F. Growth of Single-Walled Carbon Nanotubes from Sharp Metal Tips. *Small* **2009**, *5*, 2710–2715.
39. Rodríguez-Manzo, J. A.; Terrones, M.; Terrones, H.; Kroto, H. W.; Sun, L. T.; Banhart, F. *In Situ* Nucleation of Carbon Nanotubes by the Injection of Carbon Atoms into Metal Particles. *Nat. Nanotechnol.* **2007**, *2*, 307–311.
40. Ichihashi, T.; Fujita, J.-i.; Ishida, M.; Ochiai, Y. *In Situ* Observation of Carbon-Nanopillar Tubulization Caused by Liquidlike Iron Particles. *Phys. Rev. Lett.* **2004**, *92*, 215702.
41. Jensen, K.; Mickelson, W.; Han, W.; Zettl, A. Current-Controlled Nanotube Growth and Zone Refinement. *Appl. Phys. Lett.* **2005**, *86*, 173107.
42. Jin, C.; Suenaga, K.; Iijima, S. How Does a Carbon Nanotube Grow? An *In Situ* Investigation on the Cap Evolution. *ACS Nano* **2008**, *2*, 1275–1279.
43. Tang, D. M.; Liu, C.; Li, F.; Ren, W. C.; Du, J. H.; Ma, X. L.; Cheng, H. M. Structural Evolution of Carbon Microcoils Induced by a Direct Current. *Carbon* **2009**, *47*, 670–674.
44. Kyotani, T.; Tsai, L.-f.; Tomita, A. Preparation of Ultrafine Carbon Tubes in Nanochannels of an Anodic Aluminum Oxide Film. *Chem. Mater.* **1996**, *8*, 2109–2113.
45. Yu, W.-J.; Hou, P.-X.; Zhang, L.-L.; Li, F.; Liu, C.; Cheng, H.-M. Preparation and Electrochemical Property of Fe_2O_3 Nanoparticles-Filled Carbon Nanotubes. *Chem. Commun. (Cambridge, U. K.)* **2010**, *46*, 8576–8578.
46. Lolli, G.; Zhang, L.; Balzano, L.; Sakulchaicharoen, N.; Tan, Y.; Resasco, D. E. Tailoring (n,m) Structure of Single-Walled Carbon Nanotubes by Modifying Reaction Conditions and the Nature of the Support of CoMo Catalysts. *J. Phys. Chem. B* **2006**, *110*, 2108–2115.
47. Choi, H. C.; Kundaria, S.; Wang, D.; Javey, A.; Wang, Q.; Rolandi, M.; Dai, H. Efficient Formation of Iron Nanoparticle Catalysts on Silicon Oxide by Hydroxylamine for Carbon Nanotube Synthesis and Electronics. *Nano Lett.* **2002**, *3*, 157–161.
48. Ding, L.; Zhou, W.; Chu, H.; Jin, Z.; Zhang, Y.; Li, Y. Direct Preparation and Patterning of Iron Oxide Nanoparticles *via* Microcontact Printing on Silicon Wafers for the Growth

of Single-Walled Carbon Nanotubes. *Chem. Mater.* **2006**, *18*, 4109–4114.
49. Emmenegger, C.; Bonard, J. M.; Mauron, P.; Sudan, P.; Lepora, A.; Grobety, B.; Züttel, A.; Schlapbach, L. Synthesis of Carbon Nanotubes over Fe Catalyst on Aluminium and Suggested Growth Mechanism. *Carbon* **2003**, *41*, 539–547.
50. Han, S.; Yu, T.; Park, J.; Koo, B.; Joo, J.; Hyeon, T.; Hong, S.; Im, J. Diameter-Controlled Synthesis of Discrete and Uniform-Sized Single-Walled Carbon Nanotubes Using Monodisperse Iron Oxide Nanoparticles Embedded in Zirconia Nanoparticle Arrays as Catalysts. *J. Phys. Chem. B* **2004**, *108*, 8091–8095.
51. Kyotani, T.; Pradhan, B. K.; Tomita, A. Synthesis of Carbon Nanotube Composites in Nanochannels of an Aanodic Aluminum Oxide Film. *Bull. Chem. Soc. Jpn.* **1999**, *72*, 1957–1970.
52. Lin, M.; Tan, J. P. Y.; Boothroyd, C.; Loh, K. P.; Tok, E. S.; Foo, Y. L. Dynamical Observation of Bamboo-Like Carbon Nanotube Growth. *Nano Lett.* **2007**, *7*, 2234–2238.
53. Baker, R. T. K.; Barber, M. A.; Harris, P. S.; Feates, F. S.; Waite, R. J. Nucleation and Growth of Carbon Deposits from the Nickel Catalyzed Decomposition of Acetylene. *J. Catal.* **1972**, *26*, 51–62.
54. Tibbetts, G. G. Why Are Carbon Filaments Tubular? *J. Cryst. Growth* **1984**, *66*, 632–638.
55. Feng, X.; Chee, S.; Sharma, R.; Liu, K.; Xie, X.; Li, Q.; Fan, S.; Jiang, K. *In Situ* TEM Observation of the Gasification and Growth of Carbon Nanotubes Using Iron Catalysts. *Nano Res.* **2011**, *4*, 767–779.
56. Ajayan, P. M.; Marks, L. D. Quasimelting and Phases of Small Particles. *Phys. Rev. Lett.* **1988**, *60*, 585–587.
57. Ajayan, P. M.; Marks, L. D. Experimental Evidence for Quasimelting in Small Particles. *Phys. Rev. Lett.* **1989**, *63*, 279–282.
58. Okamoto, H.; Massalski, T. The Au-C (Gold-Carbon) System. *J. Phase Equilib.* **1984**, *5*, 378–379.
59. Takagi, D.; Kobayashi, Y.; Hlbirio, H.; Suzuki, S.; Homma, Y. Mechanism of Gold-Catalyzed Carbon Material Growth. *Nano Lett.* **2008**, *8*, 832–835.
60. Takagi, D.; Homma, Y.; Hibino, H.; Suzuki, S.; Kobayashi, Y. Single-Walled Carbon Nanotube Growth from Highly Activated Metal Nanoparticles. *Nano Lett.* **2006**, *6*, 2642–2645.
61. Cui, R.; Zhang, Y.; Wang, J.; Zhou, W.; Li, Y. Comparison between Copper and Iron as Catalyst for Chemical Vapor Deposition of Horizontally Aligned Ultralong Single-Walled Carbon Nanotubes on Silicon Substrates. *J. Phys. Chem. C* **2010**, *114*, 15547–15552.
62. Ding, F.; Larsson, P.; Larsson, J. A.; Ahuja, R.; Duan, H.; Rosén, A.; Bolton, K. The Importance of Strong Carbon−Metal Adhesion for Catalytic Nucleation of Single-Walled Carbon Nanotubes. *Nano Lett.* **2007**, *8*, 463–468.